Heliyon 9 (2023) e20056

Contents lists available at ScienceDirect

Heliyon

journal homepage: www.cell.com/heliyon

Computational investigation of magnetized hybrid nanofluids heat transport and flow through elongational surface with thermal radiation and wall slip

Hashim [a], Sultan Alqahtani [b], Sohail Rehman [c,*], Sultan Alshehery [b], Sehrish Bibi [d]

[a] Department of Mathematics & Statistics, The University of Haripur, 22620, Haripur, Pakistan
[b] College of Engineering, Mechanical Engineering Department, King Khalid University, Abha, Saudi Arabia
[c] Department Mechanical Engineering, School of Material Sciences and Engineering, Georgia Institute of Technology, Atlanta, GA, 30318, USA
[d] Department of Mathematics and Statistics, Riphah International University, Islamabad, Pakistan

ARTICLE INFO

Keywords:
Thermal performance
Unsteady magnetized flow
Hybrid nanofluid
Wall slip
Dual solutions
Numerical solutions

ABSTRACT

The improved thermal performance of recently discovered hybridized nanofluids has become essential in large scale thermal processes. In fact, this is highly efficient technique to introduce the thermal efficiency of tranditional heat transferring fluids. The behavior of the nanofluid can be significantly impacted by the unsteady heating and magnetic field effects that may be present in many applications. Therefore, the current study investigat the unsteady magnetized flow of hybrid nanofluid with heat transport characteristics subject to thermal radiation and slip at the surface wall. The shrinking/stretching surface is chosen as a flow source, which is frequently occure in polymer technology, which deals with the deformability of elastic sheets, and in metallurgy, where continued strips are cooled. The novel form of shrinking surface flow is fundamentally a reverse flow and exhibits physical characteristics that differ significantly from the channel flow scenario. The distinctive features of this scruinity is the use of empirical relations to approximate the optimum thermophysical attributes of a $Cu - Al_2O_3/$ water hybrid nanofluid in order to model the 2-dimensional flow past a flat shrinking/stretching sheet under the action of radiation, Lorentz forces and realastic boundary condition responses. The governing system of modelled equation are assembled using the Tiwari-Das model in conjunction with a hybrid mass-based nanofluid model. The bvp4c algorithm is employed within the computer MATLAB programme. The hybrid nanofluid flow shows conclusive improvement in the frictional coefficient and heat transport performance. However, the effectiveness the unsteadiness parameter deteriorates the heat transmission. In the contiguity of a suction parameter, multiple outcomes appear to arise for both stretched and shrinking instances. The coefficient of energy transport improves as the magnetic factor is augmented, however the skin coefficient of friction exhibits dual behavior for the second solutions. A time-dependence investigation is undertaken to figure out the reliability of the twin solutions, and it is discovered that merely one of them remains stable and aesthetically credible.

* Corresponding author.
E-mail addresses: hashim@uoh.edu.pk (Hashim), srehman34@gatceh.edu, sohail08ktk@gmail.com (S. Rehman).

https://doi.org/10.1016/j.heliyon.2023.e20056
Received 20 April 2023; Received in revised form 7 September 2023; Accepted 10 September 2023
Available online 12 September 2023

1. Introduction

Nomenclature

(x, y)	Cartesian coordinates (m)
u, v	Components of flow in x and y directions (ms^{-1})
U_w, u_∞	Sheet velocity, free stream velocity (ms^{-1})
v_w	Mass suction velocity through the sheet (ms^{-1})
L	Slip coefficient
T, T_w, T_∞	Fluid, sheet and free ambient temperature (K)
$b > 0, c$	Constants
B	Magnetic field $(Tesla)$
t	Time (sec)
λ	Stretching parameter for $\lambda > 0$ and shrinking $\lambda < 0$
(ρC_p)	Fluid heat capacitance $(J \bullet K^{-1} \bullet m^{-3})$
C_p	specific heat at constant pressure $(J \bullet kg^{-1} \bullet K^{-1})$
μ	dynamic viscosity of the fluid $(kg \bullet m^{-1} \bullet s^{-1})$
σ	electrical conductivity of the fluid $(S \bullet m^{-1})$
σ^*	Stefan-Boltzmann constant $(W \bullet m^{-2} \bullet K^{-4})$
hnf	Hybrid nanofluid
Ec	Eckert number
S	mass flux parameter
$s1$	first solid particle
Rd	Radiation parameter
ρ	density of the fluid $(kg \bullet m^{-3})$
ψ	Stream function
τ	dimensionless time variable
υ	kinematic viscosity of the fluid $(m^2 \bullet s^{-1})$
φ_1, φ_2	nanoparticle volume fractions for Al_2O_3 (alumina) and Cu (copper)
τ_w	wall shear stress $(kg \bullet m^{-1} \bullet s^{-2})$
C_f	Skin friction
q_w	Wall heat flux $(W \bullet m^{-2})$
Nu_x	Nusselt number
β	unsteadiness parameter
q_r	radiative heat flux $(W \bullet m^{-2})$
κ^*	Rosseland mean absorption coefficient (m^{-1})
f	Base function
$f(\eta)$	Dimensionless velocity
$\Theta(\eta)$	Dimensionless temperature
Pr	Prandtl number
M	Magnetic number
α_1	Slip parameter
$s2$	second solid particle
$Re^{1/2} = \sqrt{\frac{a}{\nu}}x$	Reynold number

Liquids designated as hybrid nanofluids are composed of several nanoparticles in order to expand the thermophysical characteristics of the working fluids. The properties of mono nanofluids can be customised by changing the concentration or ratio of the nanoparticles. On the other hand, monotonous nanoliquids showed consistent thermophysical characteristics in a confined assortment by utilising just one kind of nanoparticle (nonmetallic or metallic). In recent years, hybrid nanoliquids have been developed to mend the thermophysical attributes and heat transfer abilities of fluids. Due to their hydrothermal characteristics, hybrid nanoliquids have a extensive variety of solicitations in heat exchangers, heat pipes, heat sinks and solar panels. The relationships between the Nusselt number and the frictional coefficent are also referenced in several applications procedures that require heat transfer. Thermal management is a field that is constantly growing and making significant strides forward in all phase containing cooling and heating, electricity production, electronic devices, manufacturing sectors and biomedical features. Due to the component miniaturisation and exponential growth in manufacturing capabilities, the heat flux or density has significantly increased, which poses a task to the traditional chilling technologies. Exhausting a hybrid nanofluid (HNF) is primarily intended to upturn heat efficiency in a variety of

engineering and industrial processes, including the creation of sheet and rubber sheeting among other sophisticated materials. Indeed, when a stretching sheet is present, like extrusion procedures, the eminence of the closing product depends on the mass and heat transmission. Such types of fluid flow were explained by Siddheshwar et al. [1], but the flow past a stretched sheet was first demonstrated by Crane [2]. Many experts started to pay attention to fluid flow in the existence of shrinking sheets. In a theoretical examination, Mahabaleshwar et al. [3] looked at the flow of an impulsively extending sheet past an unsteady MHD laminar boundary layer. The MHD flow of viscoelastic fluid and power law models in the context of a stretched surface were both studied by Andersson et al. [4,5]. Later, a large number of researchers conducted in-depth studies on fluid flow in the existence of hybrid nanofluids and nanofluids with a different motivations, such as in the existence of radiation and mass transpiration. A nanofluid investigations was carried out with a range of boundary circumstances under the influence of a stretching sheet by Mahabaleshwar et al. [6,7]. Some researchers also studied hybrid nanofluids in addition to nanofluids. The right method of hybridization is most beneficial for the hybrid nanofluid thermal efficiency, according to research on recent developments in hybrid nanofluids by Sarkar et al. [8,9] using three distinct base fluids, including water, oil, and ethylene glycol. In the presence of a stretched sheet, Devi and Devi [10] investigated the $Cu - Al_2O_3/H_2O$ hybrid nanofluid. Both nanofluids and hybrid nanofluids have a extensive range of physical applications [11].

Potential advantages for the fluid dynamics caused by a stretched sheet can be found in the hot wire drawing, rolling, and fiber glass processing plants. Sakiadis [14] first looked into the boundary layer flow over a continuous rigid sheet drifting with a constant speed of light. Crane [2] provide ground breaking concept by providing an analalytic solution for the two-dimensional steady flow caused by a stretched sheet in a dormant fluid. After that several researcher consider the different features of stretched sheet problem and achieved normalized solutions, including Chen and Char [15], Wang [16], Gorla and Sidawi [16], Magyari and Keller [17], Andersson [18], and Ishak et al. [19]. Researchers subsequently looked into the scenario of a sheet that was shrinking rather than extending. A new kind of shrinking sheet flow that Goldstein [20] describes a backward flow. Wang [21] initially noticed the emergence of the peculiar form of flow brought on by shrinking while studying the characterestics of a liquid film on an erratic stretched surface. As an explicit solution of the Navier-Stokes equations exhbiting the steady flow past a contracting sheet was studied by Miklavi and Wang [22]. They discovered that mass suction is necessary to sustain the flow over a contracting sheet. Fang et al. [23], Fang [24], and Fang [25] examined the flow produced by a contracting sheet of power-law liquid model with constant velocity. The flow caused by a contracting sheet reveals physical characteristics that are substantially different from the flow caused by forward stretching. Numerous researchers, including [26–30] eloborates problems involving shrinking/stretced sheet with different fluids and many geometry under diverse conditions.

The primary benefit of slip mechanism may be the reduction of flow resistance in microchannels and the enhancement of the efficiency of nanoscale viscous pumps. It is important to look at various slip-related research projects, particularly to address the right level of slip velocity for significance that are also concerned with related aspects. The first scientist who look at the velocity slip influence on the boundary layer flow in a viscous fluid was Anderssonn [18]. Using the influence of radiative heat flux and mixed convection flow of the MHD carbon nanotubes (CNTs), Maraj et al. [31] investigate the analytic solution of nanofluid. In the most recent study, Nadeem and Abbas [32] examined the slipage impact of micropolar hybrid nanofluids. Muhammad et al. [33] investigated the mechanism of heat transport mechanism utilising the slip perimeter influence in the context of viscous dissipations hybrid nanoliquid, nanofluid, and working fluid on multiwalled nanotubes. Yan et al. [34] examined the dual and stability analysis for joule heating and various slip scenrio on hybrid magnetized nanofluid with the aid of a few additional variables. Moreover, comparable findings on slip conditions in the presence of hybrid nanofluids have been reported by Eid et al. [35] and Aly et al. [12]. The results of the aforementioned research investigations may serve as the initial step for engineers and scientists in anticipating and managing the velocity slip effect in the track of the appropriate application.

Traditionally, adding nanomaterials raises the rate of thermodynamic growth of the liquid flow; however, in the case of a computationally deteriorating solution, the influence is retracted, and the rate of heat transfer of a hybrid nanofluid is fewer than that of the original fluid and its nanofluid counterpart. In the light of the previous investigations, several investigators concentrated on an MHD flow over an extensible surface rather than a glaring stretch/shrinking surface, and only identified one treatment. A porous stretch/shrinking interface is important in manufacturing processes where the external surface may not be stationary, such as polymeric extruding, fluid crystal, and ceramic material production. To the extent of the expertise, no previous studies have explored the unsteady flow in hybrid nanofluid caused by linear porous stretch/shrinking sheet with magnetohydrodynamics (MHD) as part of their mathematical framework. As a result of the aforementioned knowledge gap, the ultimate purpose of this research is to create a computational model exploring the hybrid nanofluid model and perform a stability study of an unsteady MHD stagnation point flow caused by a linear permeable stretching/shrinking sheet. The Tiwari and Das [36] nanofluid model is being used in the current work to analyze the model of the time-dependent flow and heat transport of a hybrid nanofluid via a stretch/shrinking surface with wall mass suction and slip mechanism. Two distinct nanoparticles, $Cu - Al_2O_3$ are suspended in pure water to create a hybrid nanofluid. In a broader context, the favourable qualities of both materials may be enhanced by balancing out the susceptible aspect with another material using a pair of well-composed nanomaterials. Suresh et al. [37] indicated that the hybrid $Cu - Al_2O_3$/water nanoliquids is proficient of boosting the effectiveness of thermal conductivity and fluid flow resiliency, thus the $Cu - Al_2O_3$ nanoparticles were chosen for the given investigation. The MATLAB systems software bvp4c approach is used to produce problem solutions. This model used a combination method with fourth-order precision and was widely accepted due to its strong stability properties. The findings clarification is clearly reflected. Our investigation identified the fluid flow separation sites and demonstrated the distinct interactions between separate solution. Furthermore, we state that this inquiry is novel and that all numerical results achieved are unique.

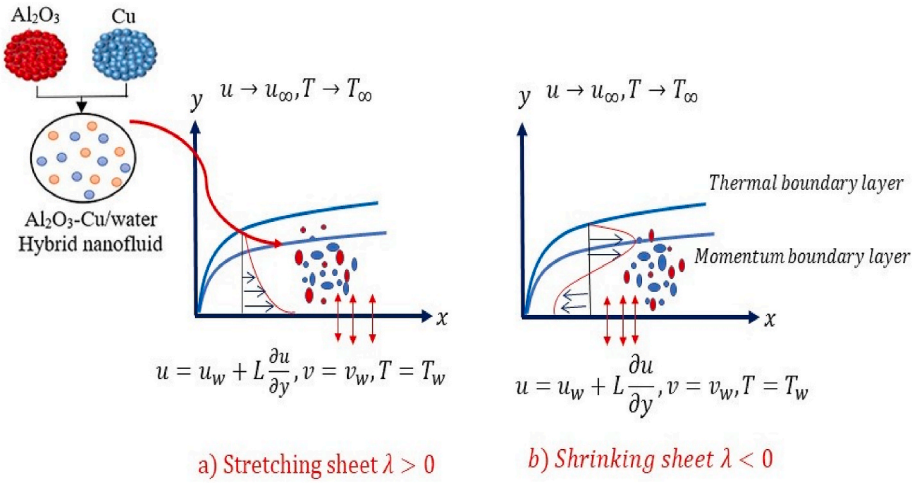

Fig. 1. Description of physical model.

2. Problem description

In this study, a stretched/shrinking surface with a sheet positioned at $y = 0$ has been used to explore the time-dependent incompressible flow and energy transfer of hybrid nanofluids. The schematic of interest in the current work is depicted in Fig. 1(a, b). Using cartesian coordinates (x, y) and boundary constraints. The x direction is aligned to the shrinking sheet and y direction is perpendicular to it. The two-dimensional flow velocities in (x, y) directionsare u and v, respectively. The surface is capable of stretching and shrinking in x direction with velocity $u_w(x, y) = \frac{U_w}{1-ct}$, where t depicts time, c means unsteadiness and $U_w = bx$. Physically, $c > 0$, promotes the external flow ability; $c < 0$ deleinate the reverses flow, and $c = 0$ conforms the inviscid steady flow. Additionally, it is simulated that the mass flow velocity is $v_w(x,y)$, with $v_w > 0$, elucidate the injection and $v_w < 0$ for suction. The fuid temperature at the wall and free stream is given by constants T_w and T_∞. The frictional dissipation and the action of radaint heat flux are also considered. A smooth transverse magnetic field with strength B additionally operates along to the y-axis. It is also expected that the hybridized nanoliquids is electrically conductive and the corresponding magnetic Reynolds number is low enough to ignore the induced magnetic field. When studying the hybrid nanofluid, it is believed that the size of the nanomaterials is homogeneous, and the influence of nanoparticle aggregation on thermophysical characteristics is ignored. The considered problem in this analysis is composed of $Cu- Al_2O_3$/water hybrid nanofluid flowing over an elongational surface, which is assumed as a two-dimensional, unsteady, incompressible and Newtonian. The base liquid and the nanoparticles are put into account while establishing thermal equilibrium.

The equations describing momentum, continuity, and heat with the initial and boundary conditions are constructed employing the Boussinesq-approximations theory. Employing Tiwari and Das model and considering the above-mentioned assumptions, the leading equations in terms of the primitive variables formulation are written as [9,38]:

$$\frac{\partial u}{\partial x}+\frac{\partial v}{\partial y}=0, \tag{1}$$

$$\frac{\partial T}{\partial t}+u\frac{\partial u}{\partial x}+v\frac{\partial v}{\partial y}=\frac{\mu_{hnf}}{\rho_{hnf}}\frac{\partial^2 u}{\partial y^2}-\frac{\sigma_{hnf}B^2u}{\rho_{hnf}}, \tag{2}$$

$$\frac{\partial T}{\partial t}+u\frac{\partial T}{\partial x}+v\frac{\partial T}{\partial y}=\frac{k_{hnf}}{(\rho c_p)_{hnf}}\frac{\partial^2 T}{\partial y^2}+\frac{\mu_{hnf}}{(\rho c_p)_{hnf}}\left(\frac{\partial u}{\partial y}\right)^2-\frac{1}{(\rho c_p)_{hnf}}\frac{\partial q_r}{\partial y}, \tag{3}$$

$$\text{At } y=0;\ v=v_w(x,t), u=\lambda u_w(x,t)+L\frac{\mu_{hnf}}{\rho_{hnf}}\frac{\partial u}{\partial y}, T=T_w, \text{for } t\geq 0, \tag{4}$$

$$\text{At } y\to\infty;\ u=0, T=T_\infty, \tag{5}$$

$$u(x,t)=0, v_w(x,y)=0, T=T_\infty, \text{for } t<0, \tag{6}$$

$$\frac{\partial T}{\partial t}+u\frac{\partial T}{\partial x}+v\frac{\partial T}{\partial y}=\frac{k_{hnf}}{(\rho c_p)_{hnf}}\frac{\partial^2 T}{\partial y^2}+\frac{\mu_{hnf}}{(\rho c_p)_{hnf}}\left(\frac{\partial u}{\partial y}\right)^2+\frac{16\sigma^* T_\infty^3}{(\rho c_p)_{hnf}3\kappa^*}\frac{\partial^2 T}{\partial y^2}, \tag{7}$$

Table 1
Thermophysical properties of the nanomaterials [12,13].

Physical Characteristic	Base fluid (water)	Al_2O_3	(Cu)
$\rho(kg.m^{-3})$	997.1	3940	8933
$c_p(J.kg^{-1}K^{-1})$	4179	765	385
$k(W.m^{-1}K^{-1})$	0.613	40	401
$\sigma(\Omega^{-1}.m^{-1})$	0.05	1×10^{-10}	5.96×10^{7}
Pr	6.2	–	–

Table 2
Theoretical relationships for the design of hybrid nanofluids physical properties.

Nanofluid attributes	Hybrid nanofuid model
Density	$\rho_{hnf} = (1-\varphi_2)[(1-\varphi_1)\rho_f + \varphi_1\rho_{s1}] + \varphi_2\rho_{s2}$
Dynamic viscosity	$\mu_{nf} = \frac{\mu_f}{(1-\varphi_1)^{2.5}(1-\varphi_2)^{2.5}}$
Heat capacitance	$(\rho C_p)_{hnf} = (1-\varphi_2)[(1-\varphi_1)(\rho C_p)_f + \varphi_1(\rho C_p)_{s1}] + \varphi_2(\rho C_p)_{s2}$
Effective thermal conductivity	$\kappa_{hnf} = \frac{k_{s1}+2k_{nf}-2\varphi_2(k_{nf}-k_{s2})}{k_{s2}+2k_{nf}+2\varphi_2(k_{nf}-k_{s2})}\kappa_{nf}$ Where $\kappa_{nf} = \frac{k_{s1}+2k_f-2\varphi_1(k_f-k_{s1})}{k_{s2}+2k_f+2\varphi_1(k_f-k_{s1})}\kappa_f$
Electrical conductivity	$\frac{\sigma_{nf}}{\sigma_f} = \frac{\sigma_{s2}+2\sigma_{bf}-2\varphi_2(\sigma_{bf}-\sigma_{s2})}{\sigma_{s2}+2\sigma_{bf}+\varphi_2(\sigma_{bf}-\sigma_{s2})}$ and $\frac{\sigma_{bf}}{\sigma_f} = \frac{\sigma_{s1}+2\sigma_f-2\varphi_1(\sigma_f-\sigma_{s1})}{\sigma_{s1}+2\sigma_f+\varphi_1(\sigma_f-\sigma_{s1})}$

where T depicts the hybrid nanofuids temperature. Furthermore, μ_{hnf} hybrid nanofuids dynamic viscosity, ρ_{hnf} density of hybrid nanofluid, k_{hnf} , and $(\rho c_p)_{hnf}$ are thermal conductivity and heat capacity of hybrid nanofluid, respectively. There mathematical and numerical expressions are given in Tables 1 and 2, respectively.

The implemented variables and relevant parameters in the simulation of non-dimensional leading equations are:

$$\eta = y\sqrt{\frac{a}{\nu_f(1-ct)}}, \psi = x\sqrt{\frac{a\nu_f}{(1-ct)}}, \Theta(\eta) = \frac{T-T_\infty}{T_w-T_\infty}, \tag{8}$$

Here, the stokes stream function ψ gives the velocity components in the following manner:

$$u = \frac{\partial\psi}{\partial y}, v = -\frac{\partial\psi}{\partial x}, \tag{9}$$

in the view of Eq. (8), the velocity component takes the following form:

$$u = xa\frac{f'(\eta)}{(1-ct)}, v = -\sqrt{\frac{a\nu_f}{(1-ct)}}f(\eta), \tag{10}$$

The equation of continuity (1), yielded as result of (9). Thus, the controlling Eqs. (2), (3) and (7) with the boundary conditions (4)–(6) reduced to the following dimensionless form in single variable η by replacing Eq. (8)– (10):

$$\frac{\mu_{hnf}}{\mu_f}f''' + \frac{\rho_{hnf}}{\rho_f}\left[ff'' - f'^2 - \beta\left(f' + \frac{\eta}{2}f''\right)\right] - Mf' = 0, \tag{11}$$

$$\Theta''\left(1+\frac{k_{hnf}}{k_f}Rd\right) + \frac{k_f}{k_{hnf}}\frac{(\rho c_p)_{hnf}}{(\rho c_p)_f}Pr\left[f\Theta' - \frac{\beta}{2}\eta\Theta'\right] + \frac{k_f}{k_{hnf}}\frac{\mu_{hnf}}{\mu_f}EcPrf''^2 = 0, \tag{12}$$

$$f(0) = S, f'(0) = \lambda + \alpha_1 f''(0), \Theta(0) = 1, \tag{13}$$

$$f(\infty) = 0, \Theta(\infty) = 0, \tag{14}$$

$$Rd = \frac{16\sigma^* T_\infty^3}{3\kappa^* k_f}, M = \frac{\sigma_f B_0^{\,2}}{a\rho_f}, Ec = \frac{(u_w)^2}{(c_p)_f(T_w-T_\infty)} = \frac{b\chi^2}{(c_p)_f(T_w-T_\infty)}, \beta = \frac{c}{b}, S = \frac{-v_w(x,t)}{\sqrt{\frac{a\nu_f}{(1-ct)}}}, Pr = \frac{\mu_f(c_p)_f}{\kappa_f}, \alpha_1 = L\sqrt{a\nu_f} > 0,$$

here, Rd elucidate the radiative variable, M the magnetic number, Ec the Eckert number, β the unsteadiness variable, S the suction parameter, Pr the Prantdl number, α_1 the slip parameter, λ depicts the stretch/shrinking factor, with $\lambda > 0$ (stretching) and $\lambda < 0$ (shrinking). χ is the specific length of the stretched or shrinked surface are emerging parameters in Eqs. (11)–(14).

2.1. Engineering parameters

The physical parameters utilized to simulate the flow are skin drag C_f and Nusselt number Nu_x, which are formulated in Eqs. (15) and (16):

$$C_f = \frac{\tau_w}{\rho_f (u_w)^2}, \mathrm{Nu_x} = \frac{x q_w}{k_f (T_w - T_\infty)}, \tag{15}$$

where the values of τ_w, the shear stress at the interface and q_w the energy flux at the wall are given by:

$$\tau_w = \mu_{hnf} \left.\frac{\partial u}{\partial y}\right|_{y=0}, q_w = -\left(k_{hnf} + \frac{16}{3}\frac{\sigma^* T_\infty^3}{\kappa^*}\right)\left.\frac{\partial T}{\partial y}\right|_{y=0}, \tag{16}$$

The dimensionless form of frictional coefficient and Nusselt number Eq. (17) and (18) are obtained using Eq. (9) as below:

$$C_f Re_{\sqrt{x}} = \frac{1}{(1-\varphi_1)^{2.5}(1-\varphi_2)^{2.5}} f''(0), \tag{17}$$

$$\frac{Nu}{Re_{\sqrt{x}}} = -\left(\frac{k_{hnf}}{k_f} + Rd\right)\Theta'(0), \tag{18}$$

3. Mathematical assessment for solutions stability

Meanwhile, we recognize the development of non-unique outcomes in the model problem Eqs. (11) and (12), we must follow the endeavors of Merill et al. [39] and Merkin [40] for their excellent innovations of the stability assessment techniques to meditate on the time-dependent flow equations in order to eventually identify an accurate and stable solution. In light of the time-dependent flow, new similarity parameters is proposed.

$$\tau = \frac{at}{(1-at)}, u = \frac{xa}{(1-at)}\frac{\partial f}{\partial \eta}(\eta,\tau), v = -\sqrt{\frac{a\nu_f}{(1-\alpha t)}} f(\eta,\tau), \eta = y\sqrt{\frac{a}{\nu_f(1-at)}}, \Theta(\eta,\tau) = \frac{T - T_\infty}{T_w - T_\infty}, \tag{19}$$

Implementing Eq. (19) into Eqs. (11) and (12), Eq. (20)–(23) takes the following form

$$\frac{\mu_{hnf}}{\mu_f}\frac{\partial^3 f}{\partial \eta^3} + \frac{\rho_{hnf}}{\rho_f}\left[f\frac{\partial^2 f}{\partial \eta^2} - \left(\frac{\partial f}{\partial \eta}\right)^2 - \beta\left(\frac{\partial f}{\partial \eta} + \frac{\eta}{2}\frac{\partial^2 f}{\partial \eta^2}\right)\right] - M\left(\frac{\partial f}{\partial \eta}\right) - \frac{\partial^2 f}{\partial \eta \partial \tau} = 0, \tag{20}$$

$$\left(1 + \frac{k_{hnf}}{k_f}Rd\right)\frac{\partial^2 \Theta}{\partial \eta^2} + \frac{k_f}{k_{hnf}}\frac{(\rho c_p)_{hnf}}{(\rho c_p)_f}\mathrm{Pr}\left[f\frac{\partial \Theta}{\partial \eta} - \frac{\beta}{2}\eta\frac{\partial \Theta}{\partial \eta} - \frac{\partial \Theta}{\partial \tau}\right] + \frac{k_f}{k_{hnf}}\frac{\mu_{hnf}}{\mu_f}\mathrm{EcPr}\left(\frac{\partial^2 f}{\partial \eta^2}\right)^2 = 0, \tag{21}$$

$$f(0,\tau) = S, \frac{\partial f}{\partial \eta}(0,\tau) = \lambda + \alpha_1 \frac{\partial^2 f}{\partial \eta^2}(0,\tau), \Theta(0,\tau) = 1, \tag{22}$$

$$f(\infty,\tau) = 0, \Theta(\infty,\tau) = 0, \tag{23}$$

according to Weidman et al. [41], to verify the stable behavior of the time-independent flow $f = f_0(\eta)$ and $\Theta = \Theta_0(\eta)$ that satisfy the problem with boundary values and boundary conditions (11–14), we write:

$$f(\eta,\tau) = f_0(\eta) + e^{-\omega t}V(\eta), \Theta(\eta,\tau) = \Theta_0(\eta) + e^{-\omega t}W(\eta), \tag{24}$$

where, ω is the eigenvalue of anonymous characteristics, where the functions $V(\eta)$ and $W(\eta)$ are comparatively minor as compared to $f_0(\eta)$ and $\Theta_0(\eta)$. The eigenvalue issues (20) and (21) with the boundary conditions (22) and (23) yield an infinite group of eigenvalues $\omega = \omega_1 < \omega_2 < \omega_3 < \ldots$ that perceive an early decline when ω_1 is constructive, while the development of disturbances is noticed when ω_1 is destructive, exposing the unbalanced flow. Moving forward by substituting (24) into (19)–(20).

$$\frac{\mu_{hnf}}{\mu_f}\frac{\partial^3 V}{\partial \eta^3} + \frac{\rho_{hnf}}{\rho_f}\left[f_0\frac{\partial^2 V}{\partial \eta^2} + V\frac{\partial^2 f_0}{\partial \eta^2} - 2\frac{\partial V}{\partial \eta}\frac{\partial f_0}{\partial \eta} - \beta\left(\frac{\partial V}{\partial \eta} + \frac{\eta}{2}\frac{\partial^2 V}{\partial \eta^2}\right)\right] - \frac{\partial^2 V}{\partial \eta \partial \tau} - M\left(\frac{\partial V}{\partial \eta}\right) + \omega\frac{\partial V}{\partial \eta} = 0, \tag{25}$$

$$\left(1 + \frac{k_{hnf}}{k_f}Rd\right)\frac{\partial^2 W}{\partial \eta^2} + \frac{k_f}{k_{hnf}}\frac{(\rho c_p)_{hnf}}{(\rho c_p)_f}\mathrm{Pr}\left[f_0\frac{\partial W}{\partial \eta} + V\frac{\partial \Theta_0}{\partial \eta} - \frac{\beta}{2}\eta\frac{\partial W}{\partial \eta} + \omega W\right] + 2\frac{k_f}{k_{hnf}}\frac{\mu_{hnf}}{\mu_f}\mathrm{EcPr}\left(\frac{\partial^2 f_0}{\partial \eta^2}\right)\frac{\partial^2 V}{\partial \eta^2} = 0, \tag{26}$$

To facilitate to pinpoint that initial development or degradation of solutions, we follow Weidman et al. [41] and retain $V = V_0$, and $W = W_0$ in Eqs. (25) and (26). As a result, we get the following streamlined eigenvalues problems.

Table 3
Evaluation of $C_f Re_{\sqrt{x}}$, when $\varphi_1 = 0$, $\varphi_2 = 0$, $M = 0$, $\beta = 0$ (stretching sheet case).

$\lambda = \lambda_c >$ 0	Bachok et al. [45]	Wang [46]	Zainal et al. [47]	Present result
0	1.2325877	1.232588	1.23258762	1.2325
0.1	1.1465610	1.146560	1.14656097	1.1465
0.2	1.0511300	1.051130	1.05112996	1.0511
0.5	0.7132949	0.713300	0.71329492	0.7132
2.0	− 1.8873066	− 1.887310	− 1.88730666	− 1.8873

Table 4
Evaluation of $C_f Re_{\sqrt{x}}$, when $\varphi_1 = 0$, $\varphi_2 = 0$, $M = 0$, $\beta = 0$ (shrinking sheet case).

$\lambda = \lambda_c <$ 0	Bachok et al. [45]		Wang [46]		Zainal et al. [47]		Present result	
	Primary solution	Secondary solution	Primary solution	Secondary solution	Primary solution	Secondary solution	Primary solution	Secondary solution
−1.00	1.3288170	0.0000000	1.32882	0.00000	1.32881684	0.00000000	1.3288	0.0000
−1.10	1.1866805	0.0492290	–	–	1.18668024	0.04922896	1.1866	0.0492
−1.15	1.0822315	0.1167022	1.08223	0.11670	1.08223112	0.11670214	1.0823	0.1167
−1.20	0.9324739	0.2336794	–	–	0.93247330	0.23364973	0.9324	0.2336
−1.2465	0.5842956	0.5542824	0.55430	–	0.58428107	0.55429619	0.5842	0.5542
−1.24657	0.5639733	–	–	–	0.57452457	0.56401151	0.5639	0.5640

$$\frac{\mu_{hnf}}{\mu_f}\frac{\partial^3 V_0}{\partial \eta^3}+\frac{\rho_{hnf}}{\rho_f}\left[f_0\frac{\partial^2 V_0}{\partial \eta^2}+V_0\frac{\partial^2 f_0}{\partial \eta^2}-2\frac{\partial V_0}{\partial \eta}\frac{\partial f_0}{\partial \eta}-\beta\left(\frac{\partial V_0}{\partial \eta}+\frac{\eta}{2}\frac{\partial^2 V_0}{\partial \eta^2}\right)\right]-\frac{\partial^2 V_0}{\partial \eta \partial \tau}-M\left(\frac{\partial V_0}{\partial \eta}\right)+\omega\frac{\partial V_0}{\partial \eta}=0, \tag{27}$$

$$\left(1+\frac{k_{hnf}}{k_f}Rd\right)\frac{\partial^2 W_0}{\partial \eta^2}+\frac{k_f}{k_{hnf}}\frac{(\rho c_p)_{hnf}}{(\rho c_p)_f}Pr\left[f_0\frac{\partial W_0}{\partial \eta}+V_0\frac{\partial \Theta_0}{\partial \eta}-\frac{\beta}{2}\eta\frac{\partial W_0}{\partial \eta}+\omega W_0\right]+2\frac{k_f}{k_{hnf}}\frac{\mu_{hnf}}{\mu_f}EcPr\left(\frac{\partial^2 f_0}{\partial \eta^2}\right)\frac{\partial^2 V_0}{\partial \eta^2}=0, \tag{28}$$

With

$$V_0(0)=0,\frac{\partial V_0}{\partial \eta}(0)-\alpha_1\frac{\partial^2 V_0}{\partial \eta^2}(0)=0,W_0(0)=0, \tag{29}$$

$$V_0(\infty)=0, W_0(\infty)=0, \tag{30}$$

To generate an envisaged spectrum of eigenvalues Eq. (27)–(30), Harris et al. [42] state that for the far field boundary requirements ($V_0(\infty)$, $W_0(\infty)$) must be undisturbed and replaced with a new condition. As a result, throughout the study, the boundary constraint $\frac{\partial V_0}{\partial \eta}(\infty)\to 0$ in Eq. (29) is substituted with a new boundary condition $\frac{\partial^2 V_0}{\partial \eta^2}(0) = 1$. The bvp4c function in Matlab is employed to execute the stability investigation in this segment. The least eigenvalue (ω) obtained may regulate the proper (physical) solution among multiple solutions.

4. Numerical algorithm

Employing the bvp4c solver, the similarity solutions are derived by solving the nonlinear ODEs Eqs. (10) and (11) with the BCs (see Eqs (12) and (13)). Shampine et al. [43] developed the bvp4c solver, which uses the Lobatto IIIa three-stage computational approach. The technique at hand is classified as finite difference [sol = bvp4c (@OdeBvp, @OdeBC, solinit, choices)] is the basic syntax of the bvp4c solver, and Eqs. (11) and (12) must be redrafted in the following codes: equations (11)–(14) are turned into first order differential equations for this purpose. The rate of convergence interval is chosen to be between 0 and 6, with $\eta_\infty = 6$. The approach has been verified through assessing our findings to earlier published work; as indicated in Table 3, there is good agreement with existing data. The absolute convergence criterion was chosen to be 10^{-6} [44]. The multiple solutions are gathered in this technique by modifying distinct initial guesses for $f'(0)$ and $\Theta(0)$, based on multiple physical characteristics. Furthermore, all contours must fulfill the far field criteria asymptotically. The boundary circumstances are carried out in this analysis for few finite value of the similarity variable η represented by η_{max}. For optimal asymptotic conduct of factors on temperature and velocity profiles, we computed $\eta_{max} = 7$, 10, and 15.

As shown in Tables 3 and 4, the confirmation of the outcomes produced is evaluated using the remarkable work of Bachok et al. [45] using the Runge-Kutta-Fehlberg (RKF) method, Wang [46] and Zainal et al. [47] used a standard (RKF-5) technique combined with the shooting mechanism. Notwithstanding the variety of boundary value problem solving techniques, it should be emphasized

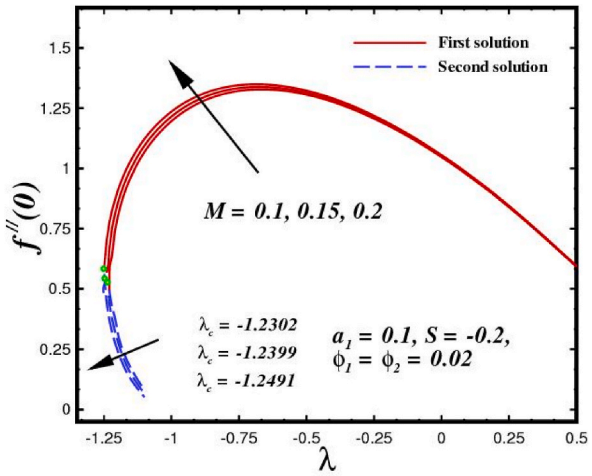

Fig. 2. $f''(0)$ variation for altered values of M and λ.

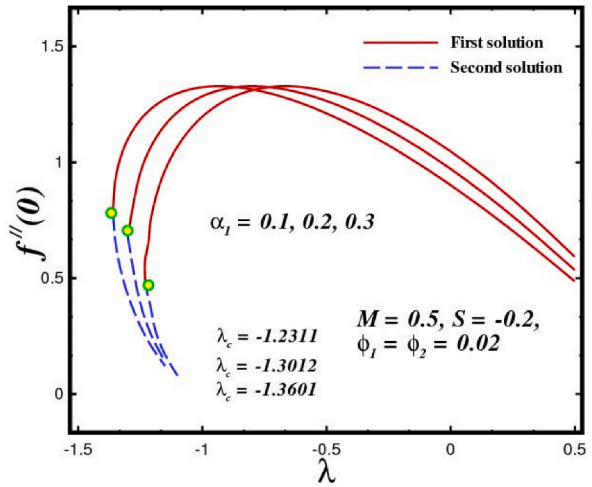

Fig. 3. $f''(0)$ variation for altered values of α_1 and λ.

that the most recent conclusions are largely in agreement with earlier ones. Thus, we can conclude that the model presented in this work is the best choice for analyzing hybridized nanofluid flow model past a stretch/shrinking surface. Based on the output of Eqs. 11)-(11, the (dual) solutions are regarded to have a particular scope of λ_c.

5. Parametric results and arguments

The normalized Eqs. (11) and (12) are solved employing the bvp4c built-in function. For a sound understanding of the details of the computational technique, it is advised to consult helpful sources like Shampine et al. [48]. Contrarily, we have chosen 100 starting meshes with 0.001 for virtual tolerance and 1×10^{-6} for entire tolerance. The character λ_c denotes a critical point or the point at which non-uniqueness solutions meet. It should be noted that there are many solutions when the sheet is shrinking ($\lambda_c < 0$), there are no dual solutions when the surface is stretching ($\lambda_c > 0$). The fluid flow disintegrates beyond the critical stage and no longer follows the flow partition theory. Although it is assumed that the primary solution is materially reliable and exist in reality, the reality of non-uniqueness solutions prompts the execution of the stability analysis in order to reach the solution that is substantially important. In the present study, the flow is described as the condition of the sheet when it is either stretching or contracting at a speed of generalized quadratic form. This section presents numerical upshots for the fluid flow (velocity profiles and frictional coefficient) and thermal features (temperature fields and Nusselt number) for various essential flow parameters. The eminent flow parameters involved in this analysis are the shrinking parameter ($-1 \leq \lambda \leq -1.3$) the magnetic parameter ($0 \leq M \leq 2$), the slip parameter ($0.1 \leq \alpha_1 \leq 0.5$), the unsteadiness parameter ($\beta = -2$), the suction parameter ($S = 2.2$), the Prandtl number ($Pr = 6.2$), Eckert number ($0.5 \leq Ec \leq 1.5$) and the radiation para-meter ($0.2 \leq Rd \leq 0.6$).

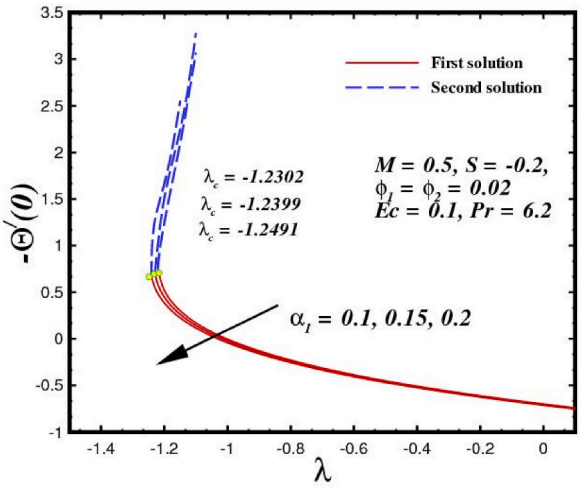

Fig. 4. Nusselt variation for altered values of α_1 and λ.

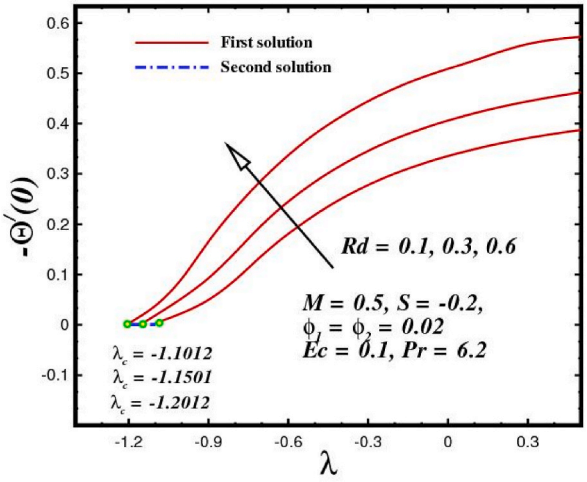

Fig. 5. Nusselt variation for altered values of *Rd* and λ.

Fig. 2 illustrates the inspiration of *M* on $C_f Re_{\sqrt{x}}$ in the presence of λ. We can see that the existence of *M* causes the demarcation of the layer at its borders where the values of λ_c are positioned marginally to the left result in drag delay. This phenomena arises because the Lorenz forces repressed the vorticity created by the shrinkage of the surface within the fluid layer, as explained by Bhattacharyya and Pop [49]. Furthermore, for the first solutions, the values of $C_f Re_{\sqrt{x}}$ increase as *M* increases, although this is clearly evident when is close to λ_c, whereas the reverse tendency is found for the secondary solutions. The multiple solutions are achieved for $\lambda > \lambda_c$, with the crucial values for $M = 0.05$, 0.1 and 0.2 being $\lambda_c = -1.2302, -1.2399, -1.2491$. Fig. 3 depicts the coefficient of skin friction $C_f Re_{\sqrt{x}}$ in relation to the stretch/shrinking parameter λ and slip velocity ($\alpha_1 = 0.1$, 0.2, 0.3) demonstrate a decrease in $C_f Re_{\sqrt{x}}$ near the interface. The similar outcomes have been published in the earlier works by Dzulkifli et al. [50]. According to Mahapatra and Nandy [51], an increase in the velocity slip indicates the statistic of the vorticity generated by the stretch or shrunk velocity decreases progressively. Although the vorticity coefficients are limited throughout the boundary region for larger elongated and shrinking parameters with the identical strained velocity of the stagnant flow, a stable solution is possible with certain broad values of λ. Furthermore, increasing the assortment of dual solutions $|\lambda_c|$ upturns indicate that increasing the range of dual solutions effectively influences the velocity slip parameter. Thus, the presence of slip α_1 control can extend the diversion of the fluid layer. Fig. 4 depicts an ascending pattern in $\frac{Nu}{Re_{\sqrt{x}}}$ when the velocity slippage parameter α_1 transpires escalating role the thermal transfer rate over the stretched and contracting sheet. These outcomes corroborate with the excellent work discussed by Mahapatra and Nandy [50] and Khashi'ie et al. [52]. Evidently, in the primary solution, the efficiency of heat transmission grows in an upward trend, but the subsequent solution provides for a downward trend as the velocity slip develops. Prior to this particular inquiry, the authors inferred from past and present findings that velocity slip significantly contributes to the augmentation of the heat transport. Fig. 5 show the effect of *Rd* parameter on local Nusselt

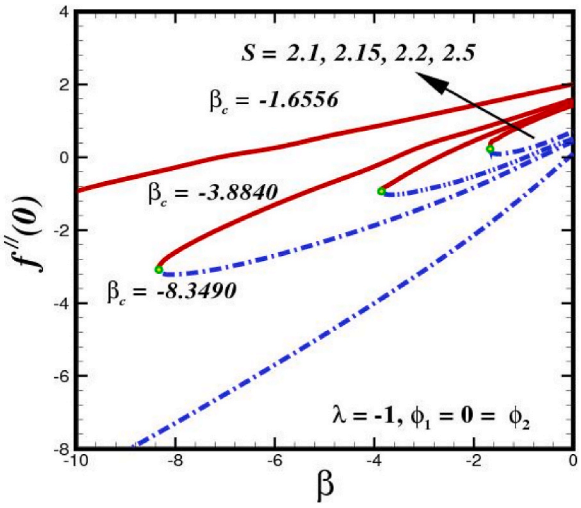

Fig. 6. $f^{'}(0)$ deviation for altered values of S and β.

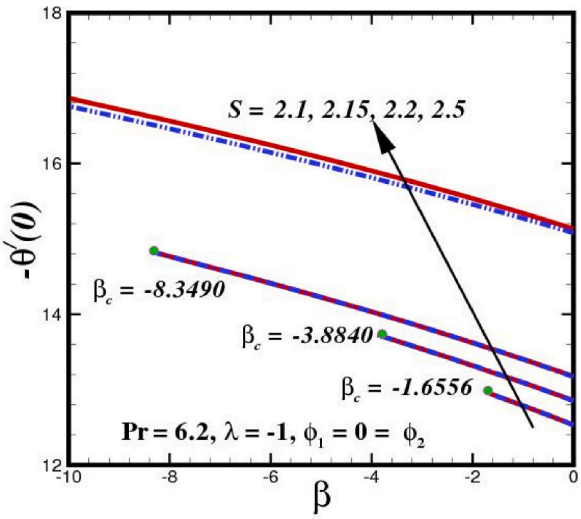

Fig. 7. Nusselt deviation for altered values of S and β.

number curves. As parameter Rd grows, the $\frac{Nu}{Re_{\sqrt{x}}}$ decreases for the initial solution while it increases for the subsequent, as illustrated in Fig. 5. As a result, increasing parameter Rd causes the heat transport rate of the hybrid nanofluid to rise. The radiative factor Rd, as described by Ref. [53], is the reverse of the Stark number, which computes the thermal radiation relative contribution to heat transport. More, substantial levels of Rd designate that heat radiation perform conduction. As a result, a higher Rd rate specifies that additional radiative heat transfer occur into the flow field, resulting in an escalation in temperature. Figs. 6 and 7 exhibits the features of skin drag friction and heat transfer rate against unsteadiness parameter β. Fig. 6 discloses that the first solution increases substantially, while the second solution retains a lowering activity as the sheet contracts. The inclusion of nanoparticle volumetric fraction in the functional fluid may also increase due to the growth in hybrid nanofluid viscosity. The impact of β on $\frac{Nu}{Re_{\sqrt{x}}}$ is displayed on Fig. 7. It is evident that as the value of β increases the declines in Nusselt can be adjudged for the first solution. It is anticipated that dual solutions (two-branches) exist when different values of the shrinkage parameter and the unsteadiness parameter are taken into account while maintaining the constant values of the other parameters. The illustrations show that multiple solutions occur with lower and upper branch for a given assortment of the unsteadiness parameter β. As earlier stated, we assume a stretch/shrinking surface with $\beta \leq 0$ indicates that the flow is decelerating. The multi solutions happen only when the value of β equals a critical number β_c. The critical value β_c is the point at which the lower and upper branch solutions encounter. Evidently are no matching solutions beyond these critical levels since the border layer splits from surface layers and solutions based on boundaries layer estimations are not achievable. The existence and addition of nanoparticles φ_1 and φ_2 should theoretically increase the kinetic energy of the fluid particles while decreasing the frictional coefficient and delaying the diverting the boundary layer, as perceived in Figs. 8 and 9. Moreover, as shown in

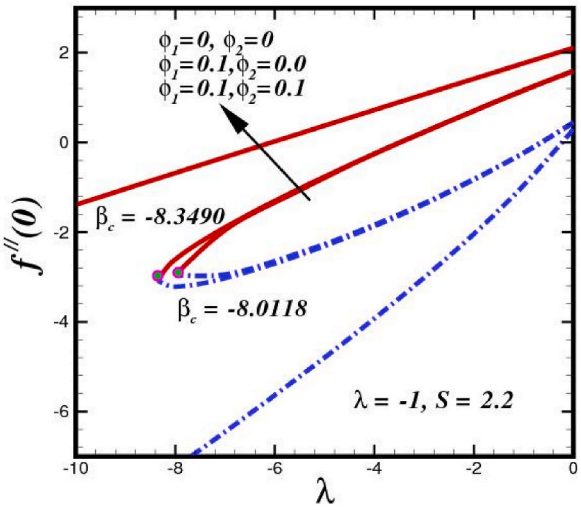

Fig. 8. $f'(0)$ variation for altered values of φ_1, φ_2 and λ.

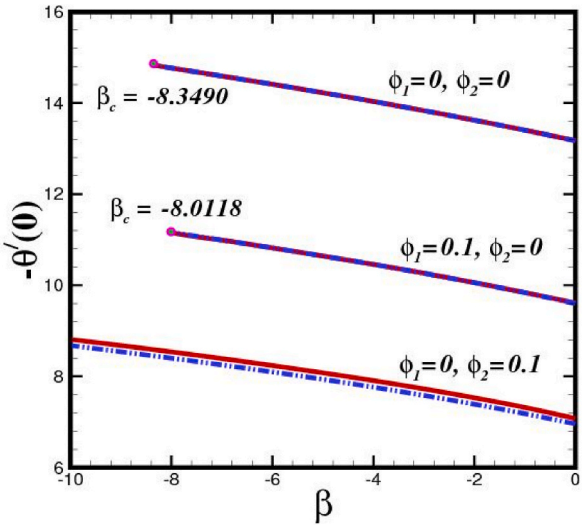

Fig. 9. Nusselt deviation for altered values of φ_1, φ_2 and β.

Fig. 8, this energy also triggers the heat transfer from fluid to the interface while also speeding up the heat transfer rate. The results indicate that when $C_f Re_{\sqrt{x}}$ develops, an increase in frictional drag might extend the boundary layer division (Fig. 9). Due to an upturn in the nanoparticle volume fraction in both working fluids, the initial solution in Fig. 10 shows an increase in the heat transport characteristic, or $\frac{Nu}{Re_{\sqrt{x}}}$, while decreasing in the other solutions. Briefly, as traditional nanofluid evolves into hybrid nanofluid, the rate of heat transmission increases. This result is because; the surface temperature falls, when φ_2 increases, the heat mechanism can be strengthened by maximizing the concentration of nanoparticles. This action backs up the pattern shown by Fig. 11, which shows the temperature changes that occur when a traditional nanofluid transforms into a hybrid nanofluid. The hybrid nanofluid thermal conductivity falls as temperature decays, improving the convective heat transfer rate over time.

To emphasize the significance of the magnetic parameter M on the flow field structure (velocity fields $f'(\eta)$ and heat transfer attribute (temperature fields $\Theta(\eta)$ for decelerating shrinking flow of hybrid nanofluids ($\beta < 0$ and $\lambda < 0$) inside the boundary layer are evaluated in Figs. 12 and 13, respectively. The ambient boundary conditions are fulfilled by the profiles solutions, confirming their reliability. As the magnetic parameter M increases, the velocity profiles gradually increases for primary branch and an opposite trend is seen for the subsequent branch. On the hand, an increase in magnetic parameter yields significant reduction in momentum boundary layer, therefore, the temperature distribution reduces in upper solution. However, in case of lower solution, the temperature profiles is seen to be an increasing function of magnetic parameter. As we can observe in the first solution, the increase in magnetic mechanism in the hybrid nanofluid system is found to enhance the thermal boundary layer thickness and decrease convective heat transfer. As a result, the rate of heat transport is reduced due to a decrease in the wall heat flux and a shrinking surface. Physically, the impedance of

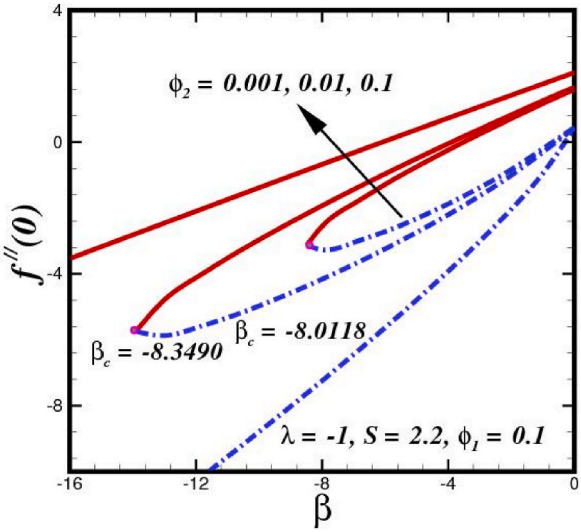

Fig. 10. $f^{'}(0)$ deviation for altered values of φ_2 and β.

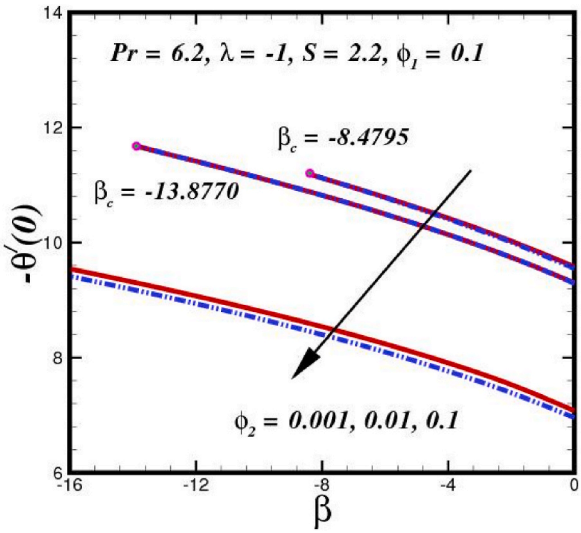

Fig. 11. Nusselt variation for altered values of φ_2 and β.

Lorentz force caused by the magnetism, increases the flow rate, enhances fluid temperature, and accelerates thermal boundary layer distinction. Figs. 14 and 15, are set up to show the distributions of velocity $f^{'}(\eta)$ and temperature $\Theta(\eta)$ for varying values of velocity slip parameter α_1. By setting the other parameters fixed, it is established in Fig. 14 that when the value of α_1 rises, the velocity slip at the wall also grows in both solutions. Additionally, compared to the upper branch velocity profiles, the lower branch velocity profiles reveal a larger boundary layer. Physically, the boundary layer bifurcation only occurs when the α_1 velocity sip parameter experiences an abrupt controlling upward or forward movement $\lambda < 0$ shrinking surface. However, for temperature profiles $\Theta(\eta)$, contradictory responses are reported when the slip parameter is elevated. In both solution profiles, the hybrid nanofluid temperature is dropped with an increase in slip parameter. Because the flow resistance is reduced as a result of the surface shrinking, a higher degree of velocity slip is required to increase flow velocity. This increases the flow velocity and vice versa. The temperature profile for both solutions diminishes as α_1 increases. In Figs. 16 and 17, the varying non-dimensional velocity and temperature distributions against distinct shrinking parameter are displayed. It is observed from the curves that hybrid nanofluid velocity reduces with higher magnitude of shrinking parameter $|\lambda|$ in upper branch, which is an inverse is noted in lower branch, as seen in Fig. 16. Similarly, a significant reduction in associated boundary layer thickness is noted in upper branch. According to this graph, the initial (stable) solution boundary layer thickness along the velocity profile grows as the shrinking parameter value increases. The second solutions show a drop in velocity and the thickness of its boundary layer due to an increase in λ. However, a significant enhancement in temperature profiles $\Theta(\eta)$ is exhibited through Fig. 17, with an increment in $|\lambda|$. The nanofluid temperature is demonstrated to increase with any increase in

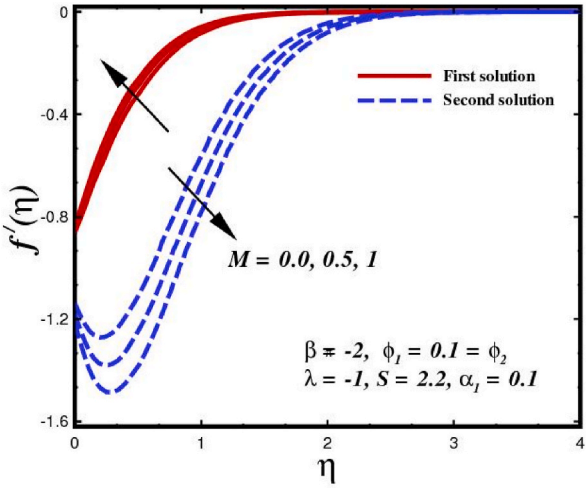

Fig. 12. Velocity $f^{'}(\eta)$ performance for altered values of M.

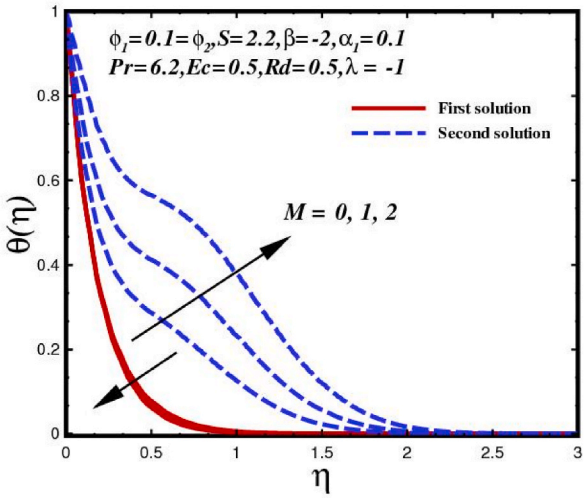

Fig. 13. Thermal performance $\Theta(\eta)$ for altered values of M.

the value of the parameter in both the first (stable) solution and the third solution, however the second solution exhibits the opposite behavior when compared to the first solutions. As shown in Figs. 18 and 19, the distributions of hybrid nanofluids temperature with variation in Eckert number *Ec* and radiation parameter *Rd* are addressed at fixed values of other parameter. It is noticeable that in both of the solutions with greater radiation parameter *Rd*, the temperature of the functional fluid and the model system temperature increase, as displayed through Fig. 18. The radiation parameter affects the distribution of heat transfer rates. The critical value does not change when this parameter increases because the laminar-turbulent flow process is not affected by the energy transport mechanism from thermal radiation. Further observations can be made by looking at the thermal progress augments as the radiation parameter increases. In general, the radiation process through the conversion of thermal energy increased the working fluid thermal performance. However, in this work, the usage of shrinking sheets affect the heat transport by the nanofluids by impairing energy transfer. The temperature of the fluid is raised physically because of the energy that the radiation applied to the nanofluid particles. The system temperature is consequently increased for hybrid nanofluid. As illustrated in Fig. 19, when the Eckert number *Ec* increases, the non-dimensional temperature profiles in both solutions display an increasing behavior. The temperatures profile and temperature boundary layer thickness for the initial and subsequent solutions grow as the Eckert number *Ec* increases. The physical justification is that when *Ec* increases, fluid viscosity gains more energy, which is converted into internal energy and, as a result, raises the distribution of temperatures.

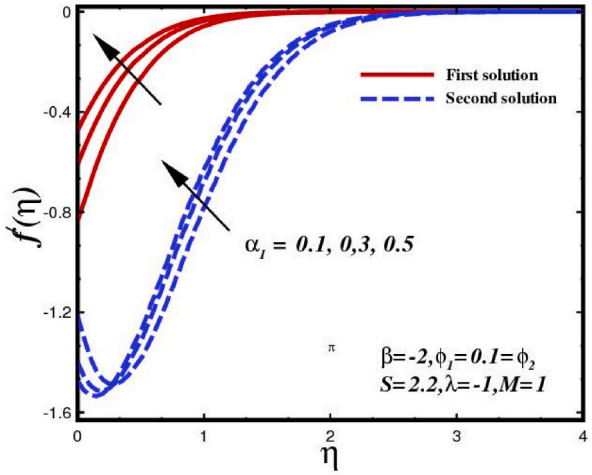

Fig. 14. Velocity $f'(\eta)$ performance for altered values of α_1.

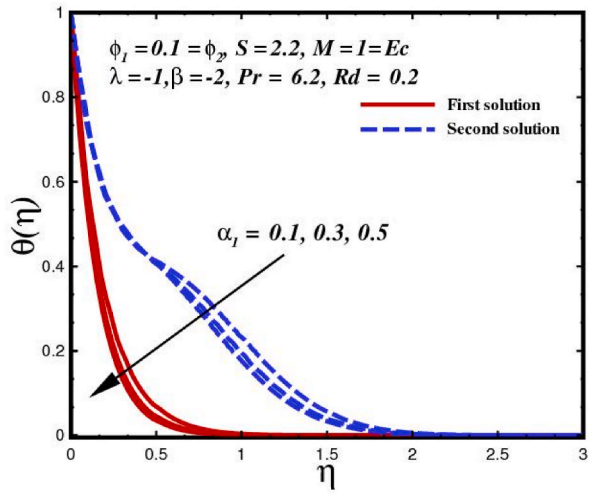

Fig. 15. Thermal performance $\Theta(\eta)$ performance for altered values of α_1.

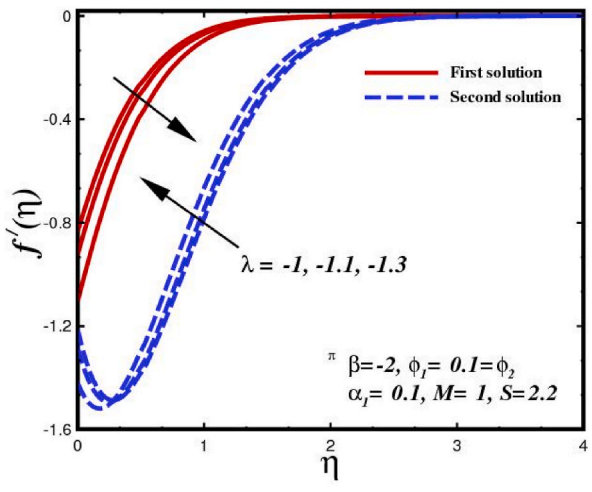

Fig. 16. Velocity $f'(\eta)$ performance for altered values of λ.

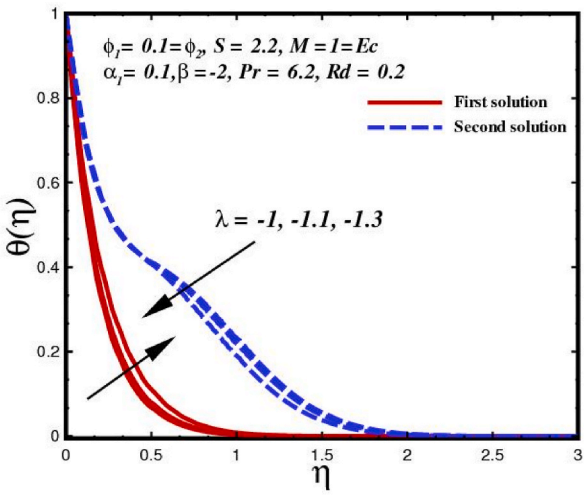

Fig. 17. Thermal performance $\Theta(\eta)$ performance for altered values of λ.

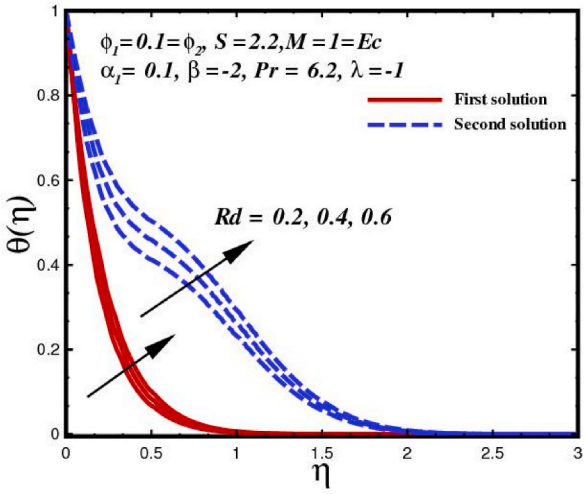

Fig. 18. Thermal performance $\Theta(\eta)$ performance for altered values of *Rd*.

6. Conclusion

The dual solutions and flow separation separations for a nanofluid flow across a linearly shrinking/stretching sheet were examined in this paper. With the integration of hybrid nanofluid and the implementation of the bvp4c technique in the MATLAB programming environment, numerical computing has been effectively implemented to carry out magnetohydrodynamics and steady flow of viscous fluid. The quadratic sheet that was stretched and then shrink with a speed of general quadratic form, which enable the fluid to move. By dispersing the Al_2O_3 (φ_1) and Cu (φ_2) nanoparticles into water with sufficient proportions of solid nanoparticle volume fractions, the hybrid alumina–copper/water nanofluid ($Cu-Al_2O_3$/water) is created. In this work, the effects of the parameters for slip, unsteadiness, magnetic parameter, and nanoparticle volume fraction were examined. For a large variety of control parameters within the hybrid $Cu-Al_2O_3$/water nanofluid, the outcomes show the incidence of non-uniqueness solutions is conclusive. Both traditional $Cu-Al_2O_3$/water nanofluid and hybrid $Cu-Al_2O_3$/water nanofluid exhibit increased values of local Nusselt number and skin friction coefficient with increasing nanoparticle volume fraction. In brief, by maximizing the concentration of nanoparticles, it has been demonstrated that the performance of heat transfer increases when the conventional nanofluid transforms into the hybrid $Cu-Al_2O_3$/water nanofluid. The skin friction coefficient of the hybrid $Cu-Al_2O_3$/water nanofluid was increased as a result of the magnetic parameter at the controlling boundary layer system, eventually. It is demonstrated that the fluid thermal state is reduced, increasing the heat transfer rate in the hybrid $Cu-Al_2O_3$/water nanofluid. The efficiency of heat transport, on the other hand, is less affected by the unsteadiness parameter. The results of this work supported the presence of first and second solutions, which are non-uniqueness solutions, in the analysis of hybrid nanofluids within a particular range of shrinking parameters λ, while a unique solution is observed

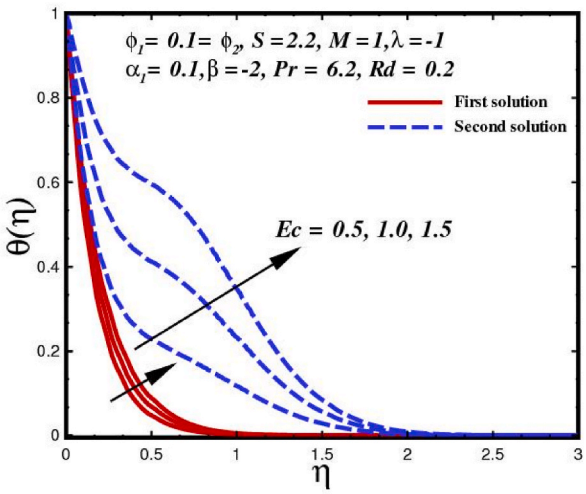

Fig. 19. Thermal performance $\Theta(\eta)$ performance for altered values of *Ec*.

in the stretched case. The hybrid $Cu-Al_2O_3$/water nanofluid delays the movement of the conducting fluid at the boundary layer when the surface is a sheet. While two distinct solutions exist, the examination of solution durability has proved the initial solution's steadiness and consistency, but the subsequent solution is unreliable and unpredictable.

Author contribution statement

Hashim: Conceived and designed the analysis; Contributed analysis tools or data. Sultan Alqahtani: Conceived and designed the analysis; Analyzed and interpreted the data. Sohail Rehman: Conceived and designed the analysis; Wrote the paper. Sultan Alshehery: Analyzed and interpreted the data; Contributed analysis tools or data. Sehrish Bibi: Contributed analysis tools or data.

Data availability statement

Data included in article/supplementary material/referenced in article.

Declaration of competing interest

The authors declare that they have no known competing financial interests or personal relationships that could have appeared to influence the work reported in this paper.

Acknowledgements

The authors extend their appreciation to the Deanship of Scientific Research at King Khalid University for funding this work through a large group research project under Grant No. RGP2/290/44.

References

[1] P.G. Siddheshwar, A. Chan, U.S. Mahabaleswar, Suction-induced magnetohydrodynamics of a viscoelastic fluid over a stretching surface within a porous medium, IMA J. Appl. Math. 79 (2014) 445–458, https://doi.org/10.1093/imamat/hxs074.
[2] L.J. Crane, Flow past a stretching plate, J. Appl. Math. Phys. 21 (1970) 645–647, https://doi.org/10.1007/BF01587695.
[3] U.S. Mahabaleshwar, K.R. Nagaraju, P.N. Vinay Kumar, D. Baleanu, G. Lorenzini, An exact analytical solution of the unsteady magnetohydrodynamics nonlinear dynamics of laminar boundary layer due to an impulsively linear stretching sheet, Continuum Mech. Therm. 29 (2017) 559–567, https://doi.org/10.1007/s00161-016-0543-9.
[4] H.I. Andersson, K.H. Bech, B.S. Dandapat, Magnetohydrodynamic flow of a power-law fluid over a stretching sheet, Int. J. Non Lin. Mech. 27 (1992) 929–936, https://doi.org/10.1016/0020-7462(92)90045-9.
[5] H.I. Andersson, MHD flow of a viscoelastic fluid past a stretching surface, Acta Mech. 95 (1992) 227–230, https://doi.org/10.1007/BF01170814.
[6] U.S. Mahabaleshwar, P.N. Vinay Kumar, M. Sheremet, Magnetohydrodynamics flow of a nanofluid driven by a stretching/shrinking sheet with suction, SpringerPlus 5 (2016) 1901, https://doi.org/10.1186/s40064-016-3588-0.
[7] L.Th Benos, N.D. Polychronopoulos, U.S. Mahabaleshwar, G. Lorenzini, I.E. Sarris, Thermal and flow investigation of MHD natural convection in a nanofluid-saturated porous enclosure: an asymptotic analysis, J. Therm. Anal. Calorim. 143 (2021) 751–765, https://doi.org/10.1007/s10973-019-09165-w.
[8] J. Sarkar, P. Ghosh, A. Adil, A review on hybrid nanofluids: recent research, development and applications, Renew. Sustain. Energy Rev. 43 (2015) 164–177, https://doi.org/10.1016/j.rser.2014.11.023.
[9] I. Waini, A. Ishak, I. Pop, Unsteady flow and heat transfer past a stretching/shrinking sheet in a hybrid nanofluid, Int. J. Heat Mass Tran. 136 (2019) 288–297, https://doi.org/10.1016/j.ijheatmasstransfer.2019.02.101.

[10] N.A.L. Aladdin, N. Bachok, I. Pop, Cu-Al2O3/water hybrid nanofluid flow over a permeable moving surface in presence of hydromagnetic and suction effects, Alex. Eng. J. 59 (2020) 657–666, https://doi.org/10.1016/j.aej.2020.01.028.
[11] U.S. Mahabaleshwar, T. Anusha, D. Laroze, N.M. Said, M. Sharifpur, An MHD flow of non-Newtonian fluid due to a porous stretching/shrinking sheet with mass transfer, Sustainability 14 (2022) 7020, https://doi.org/10.3390/su14127020.
[12] E.H. Aly, I. Pop, MHD flow and heat transfer near stagnation point over a stretching/shrinking surface with partial slip and viscous dissipation: hybrid nanofluid versus nanofluid, Powder Technol. 367 (2020) 192–205, https://doi.org/10.1016/j.powtec.2020.03.030.
[13] F.A. Soomro, M. Usman, S. El-Sapa, M. Hamid, R.U. Haq, Numerical study of heat transfer performance of MHD Al2O3-Cu/water hybrid nanofluid flow over inclined surface, Arch. Appl. Mech. 92 (2022) 2757–2765, https://doi.org/10.1007/s00419-022-02214-1.
[14] B.C. Sakiadis, Boundary-layer behavior on continuous solid surfaces: I. Boundary-layer equations for two-dimensional and axisymmetric flow, AIChE J. 7 (1961) 26–28, https://doi.org/10.1002/aic.690070108.
[15] C.-K. Chen, M.-I. Char, Heat transfer of a continuous, stretching surface with suction or blowing, J. Math. Anal. Appl. 135 (1988) 568–580, https://doi.org/10.1016/0022-247X(88)90172-2.
[16] R.S. Reddy Gorla, I. Sidawi, Free convection on a vertical stretching surface with suction and blowing, Appl. Sci. Res. 52 (1994) 247–257, https://doi.org/10.1007/BF00853952.
[17] E. Magyari, B. Keller, Exact solutions for self-similar boundary-layer flows induced by permeable stretching walls, Eur. J. Mech. B Fluid 19 (2000) 109–122, https://doi.org/10.1016/S0997-7546(00)00104-7.
[18] H.I. Andersson, Slip flow past a stretching surface, Acta Mech. 158 (2002) 121–125, https://doi.org/10.1007/BF01463174.
[19] A. Ishak, R. Nazar, UNSTEADY MIXED CONVECTION BOUNDARY LAYER FLOW DUE TO A STRETCHING VERTICAL SURFACE, 2006.
[20] S. Goldstein, On backward boundary layers and flow in converging passages, J. Fluid Mech. 21 (1965) 33–45, https://doi.org/10.1017/S0022112065000034.
[21] C.Y. Wang, Liquid film on an unsteady stretching surface, Q. Appl. Math. 48 (1990) 601–610, https://doi.org/10.1090/qam/1079908.
[22] M. Miklavčič, C. Wang, Viscous flow due to a shrinking sheet, Q. Appl. Math. 64 (2006) 283–290, https://doi.org/10.1090/S0033-569X-06-01002-5.
[23] T. Fang, W. Liang, C.F. Lee, A new solution branch for the Blasius equation—a shrinking sheet problem, Comput. Math. Appl. 56 (2008) 3088–3095, https://doi.org/10.1016/j.camwa.2008.07.027.
[24] F. Tie-Gang, Z. Ji, Y. Shan-Shan, Viscous flow over an unsteady shrinking sheet with mass transfer, Chin. Phys. Lett. 26 (2009), 014703, https://doi.org/10.1088/0256-307X/26/1/014703.
[25] T. Fang, Boundary layer flow over a shrinking sheet with power-law velocity, Int. J. Heat Mass Tran. 51 (2008) 5838–5843, https://doi.org/10.1016/j.ijheatmasstransfer.2008.04.067.
[26] U.S. Mahabaleshwar, A.B. Vishalakshi, H.I. Andersson, Hybrid nanofluid flow past a stretching/shrinking sheet with thermal radiation and mass transpiration, Chin. J. Phys. 75 (2022) 152–168, https://doi.org/10.1016/j.cjph.2021.12.014.
[27] U.S. Mahabaleshwar, E.H. Aly, T. Anusha, MHD slip flow of a Casson hybrid nanofluid over a stretching/shrinking sheet with thermal radiation, Chin. J. Phys. 80 (2022) 74–106, https://doi.org/10.1016/j.cjph.2022.06.008.
[28] V.K. Patel, J.U. Pandya, M.R. Patel, Testing the influence of TiO2− Ag/water on hybrid nanofluid MHD flow with effect of radiation and slip conditions over exponentially stretching & shrinking sheets, J. Magn. Magn Mater. 572 (2023), 170591, https://doi.org/10.1016/j.jmmm.2023.170591.
[29] T. Anusha, G.V. Bognar, U.S. Mahabaleshwar, B. Souayeh, The MHD graphene nanofluid flow between two stretching discs, Int. J. Ambient Energy 44 (2023) 780–788, https://doi.org/10.1080/01430750.2022.2142664.
[30] U.S. Mahabaleshwar, K.N. Sneha, A. Wakif, Significance of Thermo-Diffusion and Chemical Reaction on MHD Casson Fluid Flows Conveying CNTs over a Porous Stretching Sheet, Waves in Random and Complex Media, 2023, pp. 1–19, https://doi.org/10.1080/17455030.2023.2173500, 0.
[31] E.N. Maraj, N.S. Akbar, Z. Iqbal, E. Azhar, Framing the MHD mixed convective performance of CNTs in rotating vertical channel inspired by thermal deposition: closed form solutions, J. Mol. Liq. 233 (2017) 334–343, https://doi.org/10.1016/j.molliq.2017.03.041.
[32] S. Nadeem, N. Abbas, On both MHD and slip effect in micropolar hybrid nanofluid past a circular cylinder under stagnation point region, Can. J. Phys. 97 (2019) 392–399, https://doi.org/10.1139/cjp-2018-0173.
[33] K. Muhammad, T. Hayat, A. Alsaedi, B. Ahmad, S. Momani, Mixed convective slip flow of hybrid nanofluid (MWCNTs + Cu + Water), nanofluid (MWCNTs + Water) and base fluid (Water): a comparative investigation, J. Therm. Anal. Calorim. 143 (2021) 1523–1536, https://doi.org/10.1007/s10973-020-09577-z.
[34] L. Yan, S. Dero, I. Khan, I.A. Mari, D. Baleanu, K.S. Nisar, E.-S.M. Sherif, H.S. Abdo, Dual solutions and stability analysis of magnetized hybrid nanofluid with joule heating and multiple slip conditions, Processes 8 (2020) 332, https://doi.org/10.3390/pr8030332.
[35] M.R. Eid, M.A. Nafe, Thermal conductivity variation and heat generation effects on magneto-hybrid nanofluid flow in a porous medium with slip condition, Waves Random Complex Media 32 (2022) 1103–1127, https://doi.org/10.1080/17455030.2020.1810365.
[36] R.K. Tiwari, M.K. Das, Heat transfer augmentation in a two-sided lid-driven differentially heated square cavity utilizing nanofluids, Int. J. Heat Mass Tran. 50 (2007) 2002–2018, https://doi.org/10.1016/j.ijheatmasstransfer.2006.09.034.
[37] S. Suresh, K.P. Venkitaraj, P. Selvakumar, M. Chandrasekar, Synthesis of Al2O3–Cu/water hybrid nanofluids using two step method and its thermo physical properties, Colloids Surf. A Physicochem. Eng. Asp. 388 (2011) 41–48, https://doi.org/10.1016/j.colsurfa.2011.08.005.
[38] N.A. Zainal, R. Nazar, K. Naganthran, I. Pop, Slip effects on unsteady mixed convection of hybrid nanofluid flow near the stagnation point, Appl. Math. Mech.-Engl. Ed. 43 (2022) 547–556, https://doi.org/10.1007/s10483-022-2823-6.
[39] K. Merrill, M. Beauchesne, J. Previte, J. Paullet, P. Weidman, Final steady flow near a stagnation point on a vertical surface in a porous medium, Int. J. Heat Mass Tran. 49 (2006) 4681–4686, https://doi.org/10.1016/j.ijheatmasstransfer.2006.02.056.
[40] J.H. Merkin, Natural-convection boundary-layer flow on a vertical surface with Newtonian heating, Int. J. Heat Fluid Flow 15 (1994) 392–398, https://doi.org/10.1016/0142-727X(94)90053-1.
[41] P.D. Weidman, D.G. Kubitschek, A.M.J. Davis, The effect of transpiration on self-similar boundary layer flow over moving surfaces, Int. J. Eng. Sci. 44 (2006) 730–737, https://doi.org/10.1016/j.ijengsci.2006.04.005.
[42] S.D. Harris, D.B. Ingham, I. Pop, Mixed convection boundary-layer flow near the stagnation point on a vertical surface in a porous medium: brinkman model with slip, Transport Porous Media 77 (2009) 267–285, https://doi.org/10.1007/s11242-008-9309-6.
[43] L.F. Shampine, S. Thompson, Solving DDEs in Matlab, Appl. Numer. Math. 37 (2001) 441–458, https://doi.org/10.1016/S0168-9274(00)00055-6.
[44] M. Khan, Hashim, A. Hafeez, A review on slip-flow and heat transfer performance of nanofluids from a permeable shrinking surface with thermal radiation: dual solutions, Chem. Eng. Sci. 173 (2017) 1–11, https://doi.org/10.1016/j.ces.2017.07.024.
[45] N. Bachok, A. Ishak, I. Pop, Melting heat transfer in boundary layer stagnation-point flow towards a stretching/shrinking sheet, Phys. Lett. 374 (2010) 4075–4079, https://doi.org/10.1016/j.physleta.2010.08.032.
[46] C.Y. Wang, Stagnation flow towards a shrinking sheet, Int. J. Non Lin. Mech. 43 (2008) 377–382, https://doi.org/10.1016/j.ijnonlinmec.2007.12.021.
[47] N.A. Zainal, R. Nazar, K. Naganthran, I. Pop, Unsteady EMHD stagnation point flow over a stretching/shrinking sheet in a hybrid Al2O3-Cu/H2O nanofluid, Int. Commun. Heat Mass Tran. 123 (2021), 105205, https://doi.org/10.1016/j.icheatmasstransfer.2021.105205.
[48] J. Kierzenka, L.F. Shampine, A BVP solver based on residual control and the Maltab PSE, ACM Trans. Math Software 27 (2001) 299–316, https://doi.org/10.1145/502800.502801.
[49] K. Bhattacharyya, I. Pop, MHD Boundary layer flow due to an exponentially shrinking sheet, Magnetohydrodynamics 47 (2011) 337–344.
[50] T.R. Mahapatra, S.K. Nandy, Slip effects on unsteady stagnation-point flow and heat transfer over a shrinking sheet, Meccanica 48 (2013) 1599–1606, https://doi.org/10.1007/s11012-012-9688-1.

[51] N.F. Dzulkifli, N. Bachok, N.A. Yacob, N. Md Arifin, H. Rosali, Unsteady stagnation-point flow and heat transfer over a permeable exponential stretching/shrinking sheet in nanofluid with slip velocity effect: a stability analysis, Appl. Sci. 8 (2018) 2172, https://doi.org/10.3390/app8112172.
[52] N.S. Khashi'ie, N.M. Arifin, I. Pop, R. Nazar, E.H. Hafidzuddin, N. Wahi, Three-dimensional hybrid nanofluid flow and heat transfer past a permeable stretching/shrinking sheet with velocity slip and convective condition, Chin. J. Phys. 66 (2020) 157–171, https://doi.org/10.1016/j.cjph.2020.03.032.
[53] I. Waini, A. Ishak, I. Pop, Hybrid nanofluid flow and heat transfer over a nonlinear permeable stretching/shrinking surface, Int. J. Numer. Methods Heat Fluid Flow 29 (2019) 3110–3127, https://doi.org/10.1108/HFF-01-2019-0057.